PROCEEDINGS OF SCIENCE

A Review on The Presupernova Evolution of Massive Stars

Marco Limongi[1]
INAF – Osservatorio Astronomico di Roma
Via Frascati 33, I-00040, Monteporzio Catone (Rome),Italy
and
Center for Stellar and Planetary Astrophysics,
School of Mathematical Sciences, P.O. Box, 28M,
Monash University, Victoria 3800, Australia
E-mail: marco@oa-roma.inaf.it

Alessandro Chieffi
INAF – Istituto di Astrofisica Spaziale e Fisica Cosmica
Via Fosso del Cavaliere 100, 00133 Roma, Italy
and
Center for Stellar and Planetary Astrophysics,
School of Mathematical Sciences, P.O. Box, 28M,
Monash University, Victoria 3800, Australia
E-mail: alessandro.chieffi@iasf-roma.inaf.it

We review the main evolutionary properties of massive stars in the range 11-120 $M_{\odot}$ of solar metallicity during all their hydrostatic burning stages up to the presupernova phase. Special attention will be devoted to the effect of the mass loss rate during the Wolf-Rayet stages in determining the structure and the physical properties of the star prior the supernova explosion

Supernovae: lights in the darkness (XXIII Trobades Científiques de la Mediterrània)
Mao, Menorca, Spain
3-5 October, 200

[1] Speaker

PoS(SUPERNOVA)018

1. Introduction

Massive stars, exploding as core collapse supernovae, play a pivotal role in the chemical and dynamical evolution of the galaxies. In fact, they (1) provide most of the mechanical energy input into the interstellar medium via strong stellar winds and supernova explosions [1] that, in turn, induce star formation and mixing of the interstellar matter; (2) generate most of the ultraviolet ionizing radiation and power the far-infrared luminosities of galaxies through the heating of the dust; (3) contribute significantly to the integrated luminosity of the unresolved galaxies (since they are very luminous objects); (4) synthesize most of the elements (with $4<Z<38$), especially those necessary to life; (5) produce some long-lived radioactive nuclei like, e.g., ^{26}Al, ^{60}Fe and ^{44}Ti that give important information on the ongoing nucleosynthesis in the Galaxy - these gamma ray emitters constitute the main observational targets of the gamma ray satellites presently in space (i.e., INTEGRAL, RHESSI) [2]; (6) constitute the most energetic phenomenon yet found, emitting gamma-ray bursts as they collapse into black holes [3,4,5]. Moreover, the interiors of massive stars constitute invaluable laboratories with physical conditions not seen elsewhere in the universe. For example, the neutrino burst occurring few seconds prior their explosion is one of the most powerful events in the universe. Then, the understanding of the evolution and the explosion of massive stars is of paramount importance in astrophysics.

We review here the presupernova evolution, the explosion and mostly the nucleosynthesis of massive stars. In particular, we mainly focus on the advanced evolutionary phases prior to the explosion, i.e. from the core He exhaustion up to the onset of the iron core collapse. However, since the advanced burning phases strongly depends on the evolutionary history of the star during the H- and He-burning stages, here we address only the aspects of these phases relevant for the further evolution of the star up to the explosion. In particular we discuss in some detail the effect of mass loss during H- and He-burning, and in particular during the Wolf-Rayet stages, and its implications on the more advanced burning phases.

2. Definition of Massive Star

Stars are self-gravitating objects of hot plasma, emitting energy in the form of photons from the surface and/or neutrinos from the center, in hydrostatic equilibrium. The equilibrium is guaranteed by the balance between the pressure gradient – the pressure being provided by a combination of radiation, ideal gas and partially or totally degenerate electrons - and the force of gravity:

$$\frac{\partial P}{\partial r} = -\frac{GM(r)\rho(r)}{r^2} \tag{2.1}$$

where $M(r)$ is the mass interior to radius r and $\rho(r)$ is the corresponding density. The run of the central temperature as a function of the central density for a star of a given mass can be simply estimated by replacing equation (2.1) with average values between

center and surface, by adopting an equation of state for an ideal gas and by assuming a constant density model:

$$T_c \propto \rho_c^{1/3} M^2 \tag{2.2}$$

Since the star loses energy from the surface it must contract, hence the central temperature will increase following equation (2.2) until one of the above assumptions will be violated. When the central temperature is high enough the nuclear reactions take place, the nuclear energy supplies the energy lost as radiation and the gravitational contraction halts. As the nuclear fuel is exhausted, gravitational contraction and heating start again until the next nuclear fuel is ignited. On the contrary, for sufficiently high densities and low temperatures the internal structure becomes fully supported by the degenerate electrons, the contraction of the degenerate core is slowed down until it ultimately stops and the structure radiates and cools down. Following these simple considerations a massive star is defined as a star that goes through all the nuclear burning stages in a quiescent way (i.e., degeneration never takes place) and eventually explode as core collapse supernova. Typically such a behavior occurs in stars more massive than ~10 $M_\odot$.

3. Nuclear Burnings and Nucleosynthesis

During its progressive contraction and heating a massive star ignites a successive nuclear burning, either at the center or in a shell, using the products of the previous one as a fuel. Four major (core and/or shell) nuclear burnings, characterized by their principal fuel, can be identified during the evolution from the core He exhaustion up to the presupernova stage, namely, carbon, neon, oxygen and silicon burning. Typically, shell burning occurs at higher temperature and lower density compared to the central burning. In the following we will discuss the basic properties of each burning regardless whether it occurs in the center or in a shell.

3.1 Carbon Burning

Carbon burning takes place when the temperature exceeds $T \simeq 7\times10^8$ K and is triggered by the two reactions $^{12}C(^{12}C,\alpha)^{20}Ne$ and $^{12}C(^{12}C,p)^{23}Na$ that occur with almost equal probability. The free protons liberated by the $^{12}C(^{12}C,p)^{23}Na$ are mainly captured by ^{23}Na through the $^{23}Na(p,\alpha)^{20}Ne$ and $^{23}Na(p,\gamma)^{24}Mg$ reactions. As a consequence ^{23}Na is mainly converted into ^{20}Ne and ^{24}Mg . Other efficient sequences involving proton captures are $^{24}Mg(p,\gamma)^{25}Al(\beta^+)^{25}Mg$ followed by $^{25}Mg(p,\gamma)^{26}Al(\beta^+)^{26}Mg$ and $^{25}Mg(p,\gamma)^{27}Al$. At the same time most of the α-particles liberated by $^{12}C(^{12}C,\alpha)^{20}Ne$ are captured by ^{16}O, the most abundant product of He burning, through the $^{16}O(\alpha,\gamma)^{20}Ne$, and by ^{20}Ne and ^{23}Na, freshly synthesized, through the reactions $^{20}Ne(\alpha,\gamma)^{24}Mg$ and $^{23}Na(\alpha,p)^{26}Mg$. This means that the main products of carbon burning are ^{20}Ne, ^{23}Na and ^{24}Mg and a smaller amount of $^{25,26}Mg$ and ^{27}Al.

The reactions involving production and destruction of neutrons are particularly important for the s-process nucleosynthesis, i.e., the one driven by a sequence of neutron captures slower than the decay times of the unstable nuclei near the stability valley [6]. In massive stars the most efficient neutron source is the ^{22}Ne(α,n)^{25}Mg that, in turn, scales with the initial metallicity. The most efficient neutron poison is ^{20}Ne through the ^{20}Ne(n,g)^{21}Ne reaction which is, however, followed by the two reactions ^{21}Ne(α,n)^{24}Mg and ^{21}Ne(p,γ)^{22}Na. Since the first one gives back a neutron, the efficiency of ^{20}Ne as a neutron poison depends on the relative efficiency between these two reactions. Other efficient neutron poisons, with lower rates compared to the ^{20}Ne(n,γ)^{21}Ne are ^{23}Na(n,γ)^{24}Na, ^{24}Mg(n,γ)^{25}Mg, ^{25}Mg(n,γ)^{26}Mg, ^{27}Al(n,γ)^{28}Al. The rates of the neutron captures involving the so called s-process elements, i.e., elements heavier than iron, are lower than ~2 order of magnitudes compared to that of the ^{20}Ne(n,γ)^{21}Ne and typically scale inversely with the charge (Z) of the element. In fact, the most efficient neutron captures sequences are ^{57}Fe(n,γ)^{58}Fe(n,γ)^{59}Fe, ^{59}Co(n,γ)^{60}Co, ^{60}Ni(n,γ)^{61}Ni(n,γ)^{62}Ni, ^{56}Fe(n,γ)^{57}Fe, ^{62}Ni(n,γ)^{63}Ni, ^{63}Cu(n,γ)^{64}Cu, ^{65}Cu(n,γ)^{66}Cu, ^{66}Zn(n,γ)^{67}Zn(n,γ)^{68}Zn and so on, with progressively decreasing rates. The relative and absolute efficiency of all the reactions discussed so far may vary, even significantly, depending on the mass and metallicity of the star and on whether the burning occurs at the center or in a shell (see, e.g., [7] and also [2]).

3.2 Neon Burning

At C exhaustion the chemical composition is dominated by ^{16}O (left over by core He burning and survived to C burning), ^{20}Ne, ^{23}Na and ^{24}Mg (the main products of C burning). Among these nuclei, ^{16}O is the one having the lowest Coulomb barrier, but before temperatures for oxygen fusion are achieved, the photodisintegration of ^{20}Ne via ^{20}Ne(γ,α)^{16}O is activated at temperatures of the order of $T \sim 1.5\times10^{9}$ K. Most of the free α-particles released by ^{20}Ne(γ,α)^{16}O are captured by the remaining ^{20}Ne leading to ^{24}Mg through the ^{20}Ne(α,γ)^{24}Mg reaction. Some ^{24}Mg flows to ^{28,29,30}Si mainly through the sequences: ^{24}Mg(α,γ)^{28}Si, ^{24}Mg(n,γ)^{25}Mg(α,n)^{28}Si(n,γ)^{29}Si, ^{24}Mg(α, p)^{27}Al(p,γ)^{28}Si. One of the main products of C burning, ^{23}Na, is completely destroyed via ^{23}Na(α,p)^{26}Mg and ^{23}Na(p,α)^{20}Ne. Some ^{26}Mg flows to ^{29}Si and ^{27}Al via the (α,n) and (α,p) reactions. Other less efficient reactions of interest to nucleosynthesis (but not to the energy generation) are ^{28}Si(α,γ)^{32}S, and the p-, α- and n-captures on ^{29,30}Si leading to the synthesis of ^{31}P and ^{32}S.

In Ne burning, neutrons are mainly produced by ^{26}Mg(α,n)^{29}Si, ^{25}Mg(α,n)^{28}Si, and ^{29}Si(α,n)^{32}S, while they are mainly absorbed by ^{24}Mg(n,γ)^{25}Mg, ^{28}Si(n,γ)^{29}Si, ^{27}Al(n,γ)^{28}Al and ^{29}Si(n,γ)^{30}Si. The final composition after Ne burning is enhanced in ^{16}O, ^{24,25,26}Mg, ^{27}Al, ^{28,29,30}Si, and ^{31}P.

3.3 Oxygen Burning

At Neon exhaustion the most abundant isotope is ^{16}O and the temperature is $T \sim 1.9\times10^{9}$ K. At variance with ^{20}Ne, at these temperatures the oxygen fusion is

favored compared to its photodisintegration. Oxygen burning begins with the three ^{16}O fusion reactions, ^{16}O(^{16}O,p)^{31}P, ^{16}O(^{16}O,α)^{28}Si and ^{16}O(^{16}O,n)^{31}S(β^+)^{31}P. The branching ratios of these three reactions are ~60%, ~22% and ~18% respectively. ^{31}P is converted into ^{28}Si, ^{30}Si, ^{32}S and ^{34}S via ^{31}P(p,α)^{28}Si, ^{31}P(γ,p)^{30}Si, ^{31}P(α,p)^{34}S, and ^{31}P(p,γ)^{32}S. Initially, one of the major products of neon burning, ^{24}Mg, is completely converted into ^{28}Si and ^{30}Si via the sequences ^{24}Mg(α,p)^{27}Al, followed by ^{27}Al(α,p)^{30}Si and ^{27}Al(p,γ)^{28}Si, and ^{24}Mg(α,γ)^{28}Si. Some ^{28}Si flows to ^{32}S and ^{29}Si via the reactions ^{28}Si(α,γ)^{32}S and ^{28}Si(n,γ)^{29}Si. Then ^{29}Si is almost completely converted into ^{32,33}S and ^{30}Si via (α,n), (α,γ) and (n,γ) reactions. On the contrary, only a small amount of ^{32}S flows to ^{33}S, ^{35,37}Cl and ^{36,37}Ar through the sequences ^{32}S(n,γ)^{33}S, ^{34}S(α,p)^{35}Cl, ^{32}S(α,γ)^{36}Ar(n,γ)^{37}Ar(e^-,ν)^{37}Cl. Some amount of ^{35}Cl, ^{38}Ar and ^{39}K is also produced via ^{34}S(α,γ)^{38}Ar(p,γ)^{39}K and ^{34}S(p,γ)^{35}Cl. Hence the main products of Oxygen burning are ^{28,30}Si, ^{32}S, ^{34}S and ^{38}Ar. These species constitute ~98% of the final composition. However, the details of the final composition at O exhaustion (and in particular the relative abundance of the main products) can vary, even significantly, according to the temporal evolution of both temperature and density, that in turn depend on the mass of the star, and on whether the burning occurs in a convective core or in a convective shell. In Oxygen burning the high temperatures favor the photodisintegration of the heavy nuclei (above iron), that were produced during carbon and neon burning by s-process nucleosynthesis, into Fe peak nuclei. The most efficient photodisintegration reactions are ^{57}Fe(γ,n)^{56}Fe, ^{58}Fe(γ,n)^{57}Fe, ^{59}Co(γ,p)^{58}Fe, ^{64}Ni(γ,n)^{63}Ni(γ,n)^{62}Ni, ^{63}Cu(γ,p)^{62}Ni and ^{64}Cu(γ,n)^{63}Cu. During O burning some weak interactions become particularly efficient and may contribute significantly to the reduction of the electron fraction $Y_e = \sum_i X_i Z_i / A_i$ (for the first time after H burning where a substantial reduction of Y_e is due to the conversion of ^{1}H into ^{4}He). These are the electron captures ^{33}S(e^-,ν)^{33}P, ^{35}Cl(e^-,ν)^{35}S, ^{37}Ar(e^-,ν)^{37}Cl, ^{30}P(e^-,ν)^{30}Si and the beta decay ^{31}S(β^+)^{31}P. The efficiency of these reactions, and consequently the reduction of the electron fraction, significantly depends on whether the burning occurs in the center or in a shell. In general, the shell burning occurs at higher temperatures and lower densities compared to the central burning hence less electron captures occur there. Moreover the shell burning timescales are lower compared to the central burning. As a result a lower reduction of Y_e is found within the regions processed by shell oxygen burning.

3.4 From O exhaustion to Si ignition

Near the end of oxygen burning isolated groups of nuclei coupled by strong and electromagnetic reactions nearly balanced by their reverses start to form. As the temperature increases, more isolated groups form and smaller groups merge into larger ones. In particular, at oxygen exhaustion the temperature is typically of the order of $T \sim 2.5\times10^9$ K and one equilibrium cluster of isotopes, extending from A=24 to A=44, is formed. When the temperature rises to $T \sim 3.0\times10^9$ K another equilibrium cluster is formed and includes all the isotopes with A≥46. When the temperature is high enough ($T \sim 3.5\times10^9$ K) the two equilibrium clusters eventually merge into one big equilibrium cluster which includes all the isotopes heavier than ^{24}Mg (see [7] and [8] for a detailed description of this phenomenon). This is the consequence of the fact that the

reaction rate of a reverse process is proportional to the reaction rate of the forward companion multiplied by $e^{-Q/kT}$, where Q is the Q-value of the forward process and T the temperature of the plasma. When kT becomes larger than Q, the inverse process begins to be efficient and eventually to fully balance its forward companion.

3.5 Silicon Burning

Silicon burning stars when the most abundant species are ^{28}Si (~60%), ^{30}Si and ^{34}S and occurs in a completely different fashion compared to the previous nuclear burning stages. In fact, the presence of a big equilibrium cluster of isotopes with A≥24 limits the possibility of defining the leading processes driving the flow of the matter. On the contrary, ^{28}Si mainly burns by the sequence of photodisintegrations ^{28}Si(γ,α)^{24}Mg, ^{24}Mg(γ,α)^{20}Ne, ^{20}Ne(γ,α)^{16}O, ^{16}O(γ,α)^{12}C, ^{12}C($\gamma,2\alpha$)^{4}He, that are the most efficient reactions out of the equilibrium. The α particles released by this sequence add onto the big equilibrium group above ^{24}Mg and almost instantaneously the composition of the equilibrium cluster readjusts on the new equilibrium abundance of the α particles and on the new abundance of ^{28}Si. Because of the fast rates of reactions induced by alpha particles and nucleons and of photodisintegrations of nuclei within the equilibrium cluster, Si burning can be approximated by a sequence of quasi equilibrium states characterized by a ^{28}Si abundance and by an equilibrium abundance of α particles. Each equilibrium state may be well described by a gas of nuclei following the Maxwell-Boltzmann distribution, at fixed temperature, fixed density and fixed ^{28}Si mass fraction, in which each nucleus (N,Z) is at an equilibrium with ^{28}Si under the exchange of protons, neutrons and alpha particles. In such a condition the abundance of each isotope within the equilibrium cluster is given by:

$$Y(N,Z) = C(N,Z,\rho,T)\cdot Y(^{28}Si)\cdot Y_{\alpha}^{\delta_\alpha}\cdot Y_{p}^{\delta_p}\cdot Y_{n}^{\delta_n} \tag{3.1}$$

where δ_α, δ_p and δ_n specify the number of alpha, protons and neutrons in excess of the number in ^{28}Si and

$$C(N,Z,\rho,T) = (\rho N_A)^{\delta_\alpha+\delta_p+\delta_n}\frac{\omega(N,Z)}{\omega(^{28}Si)}2^{-\delta_p-\delta_n}\left(\frac{A(N,Z)}{A(^{28}Si)A(^{4}He)^{\delta_\alpha}}\right)^{\frac{3}{2}} \left(\frac{m_H kT}{2\pi\hbar^2}\right)^{-\frac{3}{2}(\delta_\alpha+\delta_p+\delta_n)} e^{\frac{Q(N,Z)}{kT}} \tag{3.2}$$

where ω is the partition function and Q(N,Z) is the energy required to decompose the nucleus (N,Z) into ^{28}Si, α's and nucleons. As the ^{28}Si mass fraction gradually decreases, these equations have the general property of favoring the more bound iron peak nuclei corresponding to the actual neutron to proton ratio, i.e. the neutron excess. If the neutron excess is very small (N~Z), the main product of Si burning would be ^{56}Ni because it has the largest binding energy per nucleon among all isotopes having N=Z. However during Si burning weak interactions (mainly electron captures) are far from

the equilibrium and drive the progressive increase of the neutronization [7]. As the neutron excess gradually increases, the more abundant isotope becomes ^{54}Fe or even ^{56}Fe. At the same time, the burning is not governed anymore only by (γ,α) photodisintegrations, but also by (p,α) and (n,α) reactions. Obviously, the preceding description was only a broad discussion of the sequence of events occurring during Si burning. A detailed computation of the nucleosynthesis during this nuclear burning requires a detailed solution of the an extended nuclear network. For the typical burning conditions in the core of a massive star the chemical composition following Si burning mainly consists of ^{56}Fe and ^{52}Cr which account for more than ~75% of the total mass.

The main products of each nuclear burning discussed above may be summarized as follows:

Fuel	**Main Prod.**	**Sec. Prod.**	**NUCLEAR CHARGE (Z)**
^{1}**H**	^{4}**He**	^{13}**C**, ^{14}**N**, ^{17}**O**	**2,7**
^{4}**He**	^{12}**C**, ^{16}**O**	^{18}**O**, ^{22}**Ne**, ***s*-proc.**	**6,8**
^{12}**C**	^{20}**Ne**, ^{23}**Na**, ^{24}**Mg**, ^{27}**Al**	^{25}**Mg**, ***s*-proc.**	**10,11,12,13**
^{20}**Ne**	^{16}**O**, ^{24}**Mg**, ^{28}**Si**	^{25,26}**Mg**, ^{27}**Al**, ^{29,30}**Si**, ^{31}**P**	**14, 15**
^{16}**O**	^{28,30}**Si**, ^{32,34}**S**, ^{38}**Ar**	**Cl, Ar, K, Ca**	**14,16,17,18, 19,20**
^{28}**Si**	^{52}**Cr**,^{54}**Fe**, ^{56}**Fe**	**Ti, V, Cr, Mn, Co, Ni**	**22,23,24,25, 26,27,28**

4. Neutrino Losses

Neutrino losses are an important aspect of the evolution of a massive star. In fact, in very hot environments there are enough photons in the Planck distribution having energies in excess of $m_e c^2$, m_e being the electron rest mass. As a consequence the creation of positron-electron pairs proceeds at a high rate. The created (e^+e^-) pairs quickly recombine and give back two photons per pair. Since the lifetime of pair annihilation is very short, the pair creation and annihilation quickly come to an equilibrium.

$$\gamma + \gamma \rightleftarrows e^+ + e^-$$

However, in this continuous back and forth exchange there is a small one-way leakage since a small fraction of (e^+e^-) recombinations result in a ($\nu_e \overline{\nu_e}$) instead of two photons.

$$\gamma + \gamma \rightleftarrows e^+ + e^- \rightarrow \nu_e + \overline{\nu_e}$$

Since the neutrinos exit the star at the speed of the light without interacting with the stellar plasma (while positrons, electrons and γ's remain trapped), this is an efficient mechanism of energy loss. The neutrino emission from pair production starts to become efficient when the central temperature exceeds $T \sim 8 \times 10^8$ K and continuously increases all along the further evolutionary phases up to the final collapse. For this reason the advanced evolutionary phases are called "neutrino dominated", i.e., before core C burning the main energy losses occur from the surface of the star through photons while in the advanced burning stages it occurs mainly from the center through neutrinos. Since the nuclear luminosity is regulated by the energy losses, i.e. it refurnishes the star of the energy lost, it closely follows the photon luminosity first and the neutrino luminosity later. When the nuclear reactions are not able to produce enough energy to fully sustain the star the contraction speeds up in order to gain the missing energy from the gravitational field. The dramatic increase of neutrino luminosity, and hence of the total luminosity ($L_{tot} = L_\gamma + L_\nu$), combined with the almost constant nuclear energy provided by each burning stage, implies a dramatic acceleration of the stellar evolution during the advanced burning stages. The lifetime of any given nuclear burning stage, in fact, can be simply estimated by the relation $\tau_{nuc} \simeq E_{nuc} M/L$. In the following table the estimated lifetimes without the contribution of the neutrinos are compared with the ones obtained by stellar evolution calculations including the neutrino emission.

Fuel	T_c (K)	ρ_c (g/cm^3)	E_{nuc} (erg/g)	Estimated Lifetime (no ν)	Real Lifetime
H	$4.1\ 10^7$	4.7	$6.44\ 10^{18}$	$2.2\ 10^7$ yr ($L_\gamma = 5 \cdot 10^{38}$)	$6.87\ 10^6$ yr ($L_{tot} = 5 \cdot 10^{38}$)
He	$2.1\ 10^8$	$7.2\ 10^2$	$8.70\ 10^{17}$	$1.6\ 10^6$ yr ($L_\gamma = 9 \cdot 10^{38}$)	$5.27\ 10^5$ yr ($L_{tot} = 9 \cdot 10^{38}$)
C	$8.3\ 10^8$	$1.7\ 10^5$	$4.00\ 10^{17}$	$6.3\ 10^5$ yr ($L_\gamma = 1 \cdot 10^{39}$)	$6.27\ 10^3$ yr $L_{tot} = 8 \cdot 10^{40}$
Ne	$1.6\ 10^9$	$2.5\ 10^6$	$1.10\ 10^{17}$	$1.7\ 10^5$ yr ($L_\gamma = 1 \cdot 10^{39}$)	190 days $L_{tot} = 2 \cdot 10^{43}$
O	$2.1\ 10^9$	$5.8\ 10^6$	$4.98\ 10^{17}$	$7.9\ 10^5$ yr ($L_\gamma = 1 \cdot 10^{39}$)	243 days $L_{tot} = 9 \cdot 10^{43}$
Si	$3.5\ 10^9$	$3.7\ 10^7$	$1.90\ 10^{17}$	$3.0\ 10^5$ yr ($L_\gamma = 1 \cdot 10^{39}$)	19 days $L_{tot} = 2 \cdot 10^{45}$

5. Presupernova Evolution

In this section we will briefly describe the presupernova evolution of mass loosing massive stars in the range 11-120 $M_\odot$ of initially solar metallicity. This discussion is

based on models presented in [2] and computed with the latest version of the FRANEC stellar evolutionary code.

5.1 Core H and core He burnings and the effect of Mass Loss.

The core H burning is the first nuclear burning stage and, in massive stars, is powered by the CNO cycle. The strong dependence of this cycle on the temperature implies the presence of a convective core that reaches its maximum extension just at the beginning of the central H burning and that then recedes in mass as the central H is burnt. Mass loss is rather efficient during this phase and increases substantially with the luminosity of the star (i.e. the initial mass). In stars more massive than ~40 $M_{\odot}$, it leads to a significant reduction of the total mass. For example, at core H exhaustion the 60 $M_{\odot}$ has a total mass of ~38 $M_{\odot}$ while the 120 $M_{\odot}$ ends the H burning with a total mass of ~56 $M_{\odot}$. The mass loss rate in this phase typically ranges from 10^{-6} $M_{\odot}$/yr, for the 40 $M_{\odot}$ to 10^{-5} $M_{\odot}$/yr for the 120 $M_{\odot}$. Most of the massive stars spend a significant fraction of their central H burning lifetime as O-type stars (i.e. stars with effective temperatures ranging between 50000 K>T_{eff}>33000 K) and the minimum mass that becomes an O-type star is ~14 $M_{\odot}$. The fraction of H burning lifetime spent by a star as an O-type star increases with the initial mass and varies from ~15%, for the 14 $M_{\odot}$ to ~80% for the 120 $M_{\odot}$. The H exhausted core (He core) that forms at the central H exhaustion scales (in mass) directly with the initial mass. It is worth noting here that the presently adopted mass loss rates in the blue supergiant phase [9,10] do not alter too much the Initial mass-He core mass relation at the core H exhaustion. For example, the He core mass of a 80 $M_{\odot}$ model at core H exhaustion without mass loss is ~26 $M_{\odot}$ while for the same model with mass loss it reduces to ~22 $M_{\odot}$, i.e., only by ~5%, in spite of the fact that the total mass is reduced to 47 $M_{\odot}$, i.e., by ~40%. On the contrary, the size of the H convective core, which in turn may be affected by the overshooting and/or semiconvection, has a strong impact on the Initial mass-He core mass relation and hence constitutes the greatest uncertainty in the computation of the core H burning phase.

At the core H exhaustion all the models move toward the red side of the HR diagram while the centre contracts until the core He burning begins. The further fate of the models is largely driven by the competition between the efficiency of mass loss in reducing the H rich envelope during the RSG phase and the core He burning timescale. Note that, as soon as the star expands and cools, the mass loss rate switches from that provided by [9,10] to that given by [11]. Stars initially less massive than ~30 $M_{\odot}$ do not loose most of their H rich mantle hence they will live up to the onset of the core collapse and explode as red supergiants. Viceversa stars initially more massive than this threshold value loose enough mass to end their life as WR stars. However, also these stars may spend a fraction of their He burning lifetime as red supergiants before becoming WR stars. The fraction of core He burning lifetime spent by one of these stars as a RSG (τ_{red}/τ_{He}) obviously depends on the efficiency of the mass loss and since it increases significantly with the luminosity (that in turn depends on the initial mass of the star), the larger the mass the higher the mass loss rate and the smaller the percentage of time spend by a star as a red supergiant. For example the 35 $M_{\odot}$ becomes a WNL star

when the central He mass fraction is 0.52 and $\tau_{red} / \tau_{He} \sim 0.38$, while in the 80 $M_\odot$ the transition from RSG to BSG occurs when the central He mass fraction is 0.95 and hence $\tau_{red} / \tau_{He} < 0.002$. The 120 $M_\odot$ never moves to the red because it becomes a WNL already during the latest stages of core H burning. It is worth noting here that when a star becomes a Wolf-Rayet, the mass loss rate typically reduces by about one order of magnitude compared to that in the RSG phase [12]. When the surface H mass fraction abundance drops below roughly 0.4 the star quickly moves to the blue side of the HR diagram and continues the core He burning as a WR star. As it is well known, central He burning occurs in a convective core whose mass size either advances in mass or remains fixed (at most). Such a behavior, typical in stars in which the He core mass does not shrink in mass during the central He burning, changes in the models in which the He core mass reduces during the central He burning (i.e. the WNE/WC/WO stars). The stars that become at least WNE WR stars (i.e., the ones having $X_{sup}<10^{-5}$ and $(C/N)_{sup}<0.1$ according to the standard definition) are those with $M \geq 35\ M_\odot$. Once the full H rich mantle is lost, the further evolution of the stellar model depends on the actual He core mass. In fact, as the He core is reduced by mass loss the star feels this reduction and tends to behave like a star of a smaller mass (i.e., a star having the same actual He core mass). Hence, the reduction of the He core (i.e. the total mass) during the core He burning has the following effects: 1) the He convective core reduces progressively in mass, 2) the He burning lifetime increases, 3) the luminosity progressively decreases, 4) the ^{12}C mass fraction at core He exhaustion is higher than it would be without mass loss and 4) the CO core at the core He exhaustion resembles that of other stars having similar He core masses independently on the initial mass of the star.

Stars with mass $M \geq 40\ M_\odot$ experience a mass loss strong enough that the total mass is decreased down to the mass coordinate marking the maximum extension of the He convective core. Once this happens, the star becomes a WC Wolf-Rayet star (i.e., when $(C/N)_{sup}>10$ according to the standard definition) and the products of core He burning are exposed to the surface and ejected into the interstellar medium through their stellar wind.

The relevance of the effects discussed so far, are very sensitive to the mass loss rate during the Wolf-Rayet stage. Figure 1 shows the CO core mass at core He exhaustion as a function of the initial mass for two different prescriptions of the mass loss during the WNE/WCO WR stages, i.e., the one provided by [12] (NL00) and the one provided by [13] (LA89), the second one being higher by about 0.2-0.6 dex on average compared to the first one. From the figure it is clear that while in the case of the NL00 mass loss rate the CO core mass preserves a clear trend with the initial mass, in the case of the LA89 mass loss rate all the models show a very similar structure that resembles that of a lower mass models. It goes without saying that models with initial mass $M < 35\ M_\odot$ do not differ between the two cases because they do not become WNE/WCO WR stars. Another important difference between models computed with these two different prescriptions for the mass loss is the trend of the central ^{12}C mass fraction at core He exhaustion with the initial mass. As for the CO core, also in this case, the LA89 models tend to behave like models having a similar final He core mass. Since the evolution of a massive star after core He burning is mainly driven by both the CO core mass and its

chemical composition (mainly the C/O ratio), it is clear that the mass loss during the WR stage is of paramount importance in determining the evolutionary properties of these stars during the more advanced burning stages and also their final fate (see below).

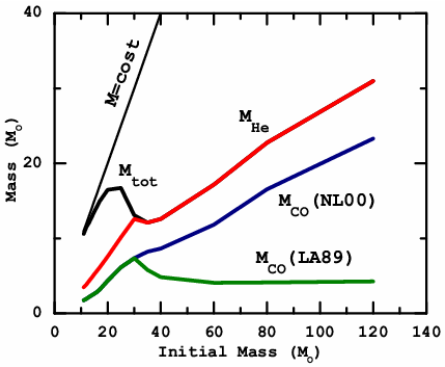

Figure 1: Total mass, He core mass and CO core mass at core He exhaustion as a function of the initial mass for two different prescriptions of the mass loss during the WR stage (see text).

Before closing this section it is worth reminding that obviously the mass loss during both the RSG and the WR phases has a strong impact on the WR lifetime and on the specific lifetimes in the various WR stages. Let us recall here few basic rules: 1) the higher the mass loss during the RSG phase the earlier the stage (the higher the central He mass fraction) at which the star enters the WR phase; 2) the higher the amount of mass lost during the WR phase the lower the actual size of the He core, the longer the He burning lifetimes and hence the longer the WR lifetime.

5.2 Advanced Burning Stages

The evolution of a massive star after core He exhaustion is mainly driven by the CO core mass and by its chemical composition, i.e., mainly the $^{12}C/^{16}O$ ratio. ^{12}C and ^{16}O constitute the basic fuel for all the nuclear burning stages following core He burning up to the explosion and hence their relative abundance determine the behavior of the star during all the advanced burning stages. The $^{12}C/^{16}O$ ratio left by core He burning mainly depends on both the treatment of convection during core He burning and the $^{12}C(\alpha,\gamma)^{16}O$ cross section [14]. Unfortunately the physics of the convective motions is still poorly known and the determination of the total cross section of the $^{12}C(\alpha,\gamma)^{16}O$ reaction is still affected by large errors, hence these two ingredients constitute the two major uncertainties in the computation of the massive star models.

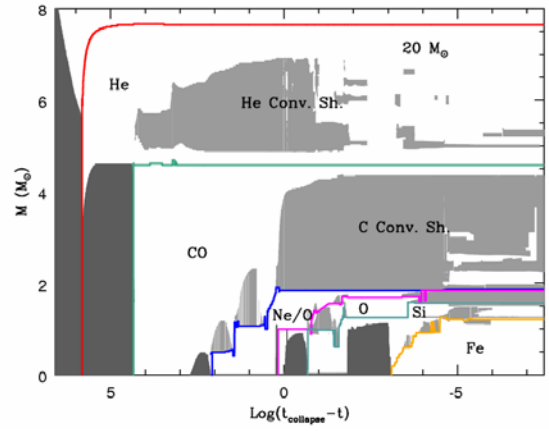

Figure 2: Convective history of a 20 $M_\odot$

Once the He is exhausted inside the CO core, the He burning shifts in a shell while the CO core contracts in order to ignite the next fuel. The advanced evolutionary phases of massive stars are characterized by four major burnings, i.e., carbon, neon, oxygen and silicon. In general each burning stage begins at the center and induces the formation of a convective core (Figure 2). The convective core increases in mass, reaches a maximum and then disappears as the nuclear fuel

is exhausted. The only exception to this general rule is core C burning that in the more massive stars (M>20 $M_\odot$) occurs in a radiative environment due to the low ^{12}C mass fraction left by core He burning. Hence the limiting mass between stars burning C in a convective core and those in which C burning occurs in a radiative environment is sensitive to this quantity that, in turn, depends on both the treatment of convection and the $^{12}C(\alpha,\gamma)^{16}O$ (see above).

Once the nuclear fuel is exhausted at the center, the burning shifts into a shell which in general is efficient enough to induced the formation of a convective zone above it (Figure 2). Once the convective zone forms, the advancing of the shell stops and the burning proceeds within the convective shell. When the nuclear fuel is exhausted within all the convective zone, the burning shell quickly shifts outward in mass, where the main fuel is more abundant and eventually another convective zone forms. By the way, two successive convective shells may also partially overlap in mass and this may have some impact on the local nucleosynthesis. The details of this general behavior, i.e. number of convective zones formed in each burning stage and their overlap, depend on both the mass of the CO core (and hence the mass of the star) and its chemical composition. In general, one to four carbon convective shells and two to three convective shell episodes for each of the neon, oxygen and silicon burnings occur. The number of C convective shells increases as the mass of the CO core decreases. For example in the 20 $M_\odot$ model (CO core of 1.74 $M_\odot$) three C convective shells form (Figure 2) while in the 60 $M_\odot$ model (CO core of 11.82 $M_\odot$) only one convective zone forms.

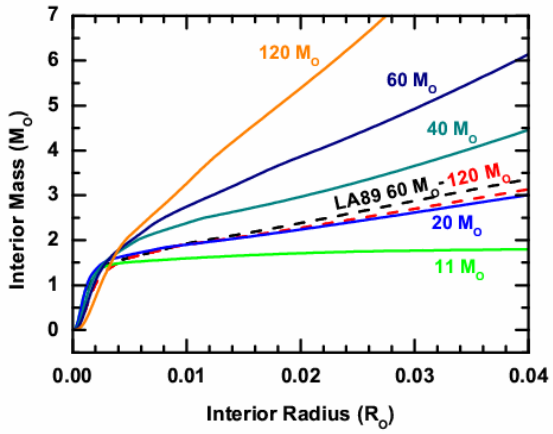

Figure 3: M-R relation for a subset of massive star models at the presupernova stage. The solid lines refer to the NL00 models while the dashed lines to the LA89 models respectively.

The complex interplay among the shell nuclear burnings and the timing of the convective zones determines in a direct way the distribution of the chemical composition and the mass-radius (M-R) relation of the star at the presupernova stage. The M-R relation is extremely important for the explosive nucleosynthesis [2,15]. In general, the more efficient is the nuclear burning (i.e., the higher is the ^{12}C mass fraction left by core He burning), the higher is the number of the convective zones and the earlier is their formation, the slower is the contraction of the CO core and the shallower is the final M-R relation. This means that the higher is the mass of the CO core, the more compact is the structure at the presupernova stage. In general the mass of the CO core scales directly with the mass, but if the mass loss is so strong to significantly reduce the He core during core He burning, this scaling could not be preserved anymore (Figure 1). The different scaling of the CO core mass with the initial mass directly reflects on the scaling between the initial mass and the final M-R relation. Figure 3 clearly shows that for the NL00 models the larger is the initial mass the more

compact is the presupernova structure while, on the contrary, all the LA89 models have a very similar M-R relation at the presupernova stage. This is the consequence of the fact that the NL00 mass loss preserves a direct scaling between the initial mass and the CO core mass while, on the contrary, the LA89 mass loss is so strong that all the LA89 models converge toward a very similar structure. By the way, all the LA89 models have a CO core mass similar to that of the 20 $M_{\odot}$ computed with the NL00 mass loss. As a consequence all the LA89 models develop a final M-R relation close to that of the 20 $M_{\odot}$ NL00 model.

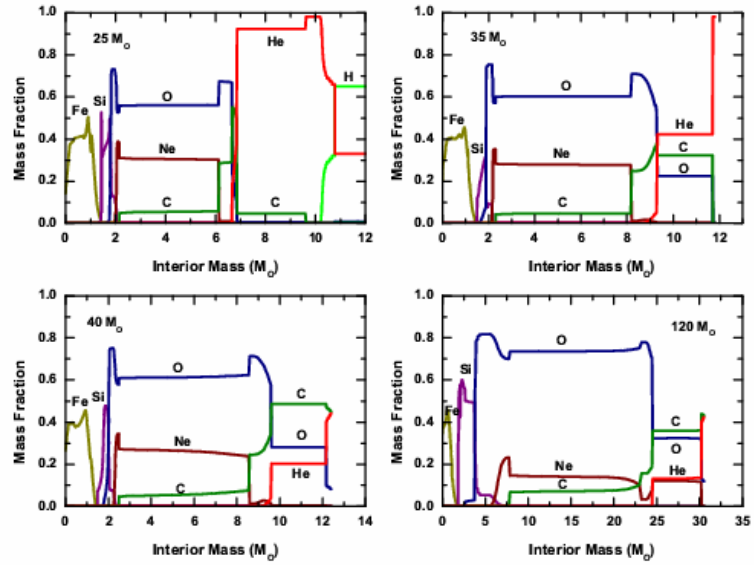

Figure 4: Presupernova distribution of the most abundant chemical species for a selected number of massive star models.

The distribution of the most abundant chemical species at the presupernova stage is shown in Figure 4 for some selected NL00 models. The 25 $M_{\odot}$ can be taken as representative of all the models in which the mass loss does not play a crucial role. On the contrary, the effect of mass loss is readily evident in the more massive stars. In general the pre-supernova star consists of an iron core of mass in the range between ~1.2 and ~1.8 $M_{\odot}$, the higher is the mass the higher is the iron core mass, surrounded by active burning shells located at the base of zones loaded in the main products of silicon, oxygen, neon, carbon, helium and hydrogen burnings, i.e., the classical "onion structure". Thus, each zone keeps memory of the nucleosynthesis produced by the various central and/or shell burnings occurring either in a radiative environment or in a convective zone.

6. Summary and Conclusion

Summarizing, stars with initial solar metallicity behave as follows (at least in the present scenario). Stars with initial mass $M < 30\ M_{\odot}$ retain a substantial fraction of their H rich envelope hence they will explode as RSG and will show the typical Type II-P SN display. On the contrary stars above this limit loose all their H rich envelope and will explode as BSG, showing either a Type Ib or a Type Ic SN display, depending on the composition of the envelope. In particular, in stars with initial mass $M < 40\ M_{\odot}$ the envelope is dominated by He, hence these stars will likely explode as Type Ib SNe. On the contrary, in stars with initial mass $M \geq 40\ M_{\odot}$ the envelope is dominated by ^{12}C

and ^{16}O and hence these stars will likely explode as Type Ic SNe. Finally, by adopting a standard Salpeter IMF we find that the ratio between SNIb/c and SNII is ~0.22, that is consistent with the observed SN rates [16].

Acknowledgement

M.L. warmly thanks Jordi Isern for the kind invitation to this meeting in Menorca.

References

[1] D.C. Abbott. Baggins, *ApJ* **1982** (263) 723

[2] M. Limongi, A. Chieffi, *ApJ* **2006** (647) 483

[3] S.E. Woosley, *ApJ* **1993** (405) 273

[4] H.A. Bethe, J.R. Wilson, *ApJ* **1985** (295) 14

[5] P.A. Price et al., *ApJL* **1985** (572) L51

[6] E.M. Burbidge, G.R. Burbidge, W.A. Fowler, F. Hoyle, *Rev. Mod. Phys.* **1957** (29) 547

[7] M. Limongi, O. Straniero, A. Chieffi, *ApJS* **2000** (129) 629

[8] A. Chieffi, M. Limongi, O. Straniero, *ApJ* **1998** (502) 737

[9] J.S. Vink, A. De Koter, H.J.G.L.M. Lamers, *AA* **2001** (369) 574

[10] J.S. Vink, A. De Koter, H.J.G.L.M. Lamers, *AA* **2000** (362) 295

[11] C. de Jager, H. Nieuwenhuijzen, K. A. van der Hucht, *AAS* **1988** (72) 259

[12] T. Nugis, H.J.G.L.M. Lamers, *AA* **2000** (360) 227

[13] N. Langer, *AA* **1988** (220) 135

[14] G. Imbriani, M. Limongi, L. Gialanella, F. Terrasi, O. Straniero, A. Chieffi, *ApJ* **2001** (558) 903

[15] M. Limongi, A. Chieffi, *ApJ* **2003** (592) 404

[16] E. Cappellaro, M. Turatto, in *The influence of binaries on stellar population studies*, Dordrecht: Kluwer Academic Publishers, **2001**, xix, 582 p. Astrophysics and space science library (ASSL), Vol. 264, p.199